

Solar  $^8\text{B}$  and *hep* Neutrino Measurements from 1258 Days of Super-Kamiokande Data

The Super-Kamiokande Collaboration

S. Fukuda<sup>1</sup>, Y. Fukuda<sup>1</sup>, M. Ishitsuka<sup>1</sup>, Y. Itow<sup>1</sup>, T. Kajita<sup>1</sup>, J. Kameda<sup>1</sup>, K. Kaneyuki<sup>1</sup>, K. Kobayashi<sup>1</sup>, Y. Koshio<sup>1</sup>, M. Miura<sup>1</sup>, S. Moriyama<sup>1</sup>, M. Nakahata<sup>1</sup>, S. Nakayama<sup>1</sup>, A. Okada<sup>1</sup>, N. Sakurai<sup>1</sup>, M. Shiozawa<sup>1</sup>, Y. Suzuki<sup>1</sup>, H. Takeuchi<sup>1</sup>, Y. Takeuchi<sup>1</sup>, T. Toshito<sup>1</sup>, Y. Totsuka<sup>1</sup>, S. Yamada<sup>1</sup>, S. Desai<sup>2</sup>, M. Earl<sup>2</sup>, E. Kearns<sup>2</sup>, M.D. Messier<sup>2</sup>, K. Scholberg<sup>2,\*</sup>, J.L. Stone<sup>2</sup>, L.R. Sulak<sup>2</sup>, C.W. Walter<sup>2</sup>, M. Goldhaber<sup>3</sup>, T. Barszczak<sup>4</sup>, D. Casper<sup>4</sup>, W. Gajewski<sup>4</sup>, W.R. Kropp<sup>4</sup>, S. Mine<sup>4</sup>, D.W. Liu<sup>4</sup>, L.R. Price<sup>4</sup>, M.B. Smy<sup>4</sup>, H.W. Sobel<sup>4</sup>, M.R. Vagins<sup>4</sup>, K.S. Ganezer<sup>5</sup>, W.E. Keig<sup>5</sup>, R.W. Ellsworth<sup>6</sup>, S. Tasaka<sup>7</sup>, A. Kibayashi<sup>8</sup>, J.G. Learned<sup>8</sup>, S. Matsuno<sup>8</sup>, D. Takemori<sup>8</sup>, Y. Hayato<sup>9</sup>, T. Ishii<sup>9</sup>, T. Kobayashi<sup>9</sup>, K. Nakamura<sup>9</sup>, Y. Obayashi<sup>9</sup>, Y. Oyama<sup>9</sup>, A. Sakai<sup>9</sup>, M. Sakuda<sup>9</sup>, M. Kohama<sup>10</sup>, A.T. Suzuki<sup>10</sup>, T. Inagaki<sup>11</sup>, T. Nakaya<sup>11</sup>, K. Nishikawa<sup>11</sup>, T.J. Haines<sup>12,d</sup>, E. Blaufuss<sup>13,14</sup>, S. Dazeley<sup>13</sup>, K.B. Lee<sup>13,†</sup>, R. Svoboda<sup>13</sup>, M.L. Chen<sup>14</sup>, J.A. Goodman<sup>14</sup>, G. Guillian<sup>14</sup>, G.W. Sullivan<sup>14</sup>, D. Turcan<sup>14</sup>, A. Habig<sup>15</sup>, J. Hill<sup>16</sup>, C.K. Jung<sup>16</sup>, K. Martens<sup>16,‡</sup>, M. Malek<sup>16</sup>, C. Mauger<sup>16</sup>, C. McGrew<sup>16</sup>, E. Sharkey<sup>16</sup>, B. Viren<sup>16</sup>, C. Yanagisawa<sup>16</sup>, C. Mitsuda<sup>17</sup>, K. Miyano<sup>17</sup>, C. Saji<sup>17</sup>, T. Shibata<sup>17</sup>, Y. Kajiyama<sup>18</sup>, Y. Nagashima<sup>18</sup>, K. Nitta<sup>18</sup>, M. Takita<sup>18</sup>, M. Yoshida<sup>18</sup>, H.I. Kim<sup>19</sup>, S.B. Kim<sup>19</sup>, J. Yoo<sup>19</sup>, H. Okazawa<sup>20</sup>, T. Ishizuka<sup>21</sup>, M. Etoh<sup>22</sup>, Y. Gando<sup>22</sup>, T. Hasegawa<sup>22</sup>, K. Inoue<sup>22</sup>, K. Ishihara<sup>22</sup>, T. Maruyama<sup>22</sup>, J. Shirai<sup>22</sup>, A. Suzuki<sup>22</sup>, M. Koshihara<sup>23</sup>, Y. Hatakeyama<sup>24</sup>, Y. Ichikawa<sup>24</sup>, M. Koike<sup>24</sup>, K. Nishijima<sup>24</sup>, H. Fujiyasu<sup>25</sup>, H. Ishino<sup>25</sup>, M. Morii<sup>25</sup>, Y. Watanabe<sup>25</sup>, U. Golebiewska<sup>26</sup>, D. Kielczewska<sup>26,4</sup>, S.C. Boyd<sup>27</sup>, A.L. Stachyra<sup>27</sup>, R.J. Wilkes<sup>27</sup>, K.K. Young<sup>27,§</sup>

<sup>1</sup> Institute for Cosmic Ray Research, University of Tokyo, Kashiwa, Chiba 277-8582, Japan<sup>2</sup> Department of Physics, Boston University, Boston, MA 02215, USA<sup>3</sup> Physics Department, Brookhaven National Laboratory, Upton, NY 11973, USA<sup>4</sup> Department of Physics and Astronomy, University of California, Irvine, Irvine, CA 92697-4575, USA<sup>5</sup> Department of Physics, California State University, Dominguez Hills, Carson, CA 90747, USA<sup>6</sup> Department of Physics, George Mason University, Fairfax, VA 22030, USA<sup>7</sup> Department of Physics, Gifu University, Gifu, Gifu 501-1193, Japan<sup>8</sup> Department of Physics and Astronomy, University of Hawaii, Honolulu, HI 96822, USA<sup>9</sup> Institute of Particle and Nuclear Studies, High Energy Accelerator Research Organization (KEK), Tsukuba, Ibaraki 305-0801, Japan<sup>10</sup> Department of Physics, Kobe University, Kobe, Hyogo 657-8501, Japan<sup>11</sup> Department of Physics, Kyoto University, Kyoto 606-8502, Japan<sup>12</sup> Physics Division, P-23, Los Alamos National Laboratory, Los Alamos, NM 87544, USA<sup>13</sup> Department of Physics and Astronomy, Louisiana State University, Baton Rouge, LA 70803, USA<sup>14</sup> Department of Physics, University of Maryland, College Park, MD 20742, USA<sup>15</sup> Department of Physics, University of Minnesota Duluth, MN 55812-2496, USA<sup>16</sup> Department of Physics and Astronomy, State University of New York, Stony Brook, NY 11794-3800, USA<sup>17</sup> Department of Physics, Niigata University, Niigata, Niigata 950-2181, Japan<sup>18</sup> Department of Physics, Osaka University, Toyonaka, Osaka 560-0043, Japan<sup>19</sup> Department of Physics, Seoul National University, Seoul 151-742, Korea<sup>20</sup> International and Cultural Studies, Shizuoka Seika College, Yaizu, Shizuoka, 425-8611, Japan<sup>21</sup> Department of Systems Engineering, Shizuoka University, Hamamatsu, Shizuoka 432-8561, Japan<sup>22</sup> Research Center for Neutrino Science, Tohoku University, Sendai, Miyagi 980-8578, Japan<sup>23</sup> The University of Tokyo, Tokyo 113-0033, Japan<sup>24</sup> Department of Physics, Tokai University, Hiratsuka, Kanagawa 259-1292, Japan<sup>25</sup> Department of Physics, Tokyo Institute of Technology, Meguro, Tokyo 152-8551, Japan<sup>26</sup> Institute of Experimental Physics, Warsaw University, 00-681 Warsaw, Poland<sup>27</sup> Department of Physics, University of Washington, Seattle, WA 98195-1560, USA

Solar neutrino measurements from 1258 days of data from the Super-Kamiokande detector are presented[? ]. The measurements are based on recoil electrons in the energy range 5.0–20.0 MeV. The measured solar neutrino flux is  $2.32 \pm 0.03$  (stat.)  $^{+0.08}_{-0.07}$  (sys.)  $\times 10^6 \text{ cm}^{-2} \text{ s}^{-1}$ , which is  $45.1 \pm 0.5$  (stat.)  $^{+1.6}_{-1.4}$  (sys.)% of that predicted by the BP2000 SSM. The day *vs* night flux asymmetry  $(\Phi_n - \Phi_d)/\Phi_{\text{average}}$  is  $0.033 \pm 0.022$  (stat.)  $^{+0.013}_{-0.012}$  (sys.). The recoil electron energy spectrum is consistent with no spectral distortion ( $\chi^2/d.o.f. = 19.0/18$ ). The seasonal variation of the flux is consistent with that expected from the eccentricity of the Earth's orbit ( $\chi^2/d.o.f. = 3.7/7$ ). For the *hep* neutrino flux, we set a 90% C.L. upper limit of  $40 \times 10^3 \text{ cm}^{-2} \text{ s}^{-1}$ , which is 4.3 times the BP2000 SSM prediction.

<sup>22</sup>This preprint is almost identical to the report submitted to Phys-

ical Review Letter. We have added to this preprint a few tables of

Solar neutrinos have been detected using chlorine-, gallium-, and water-based detectors [1, 2, 3, 4, 5]; all have measured significantly lower solar neutrino flux than predicted by Standard Solar Models (SSMs) [6, 7, 8]. This disagreement between the measured and expected solar neutrino flux, known as the “solar neutrino problem”, is generally believed to be due to neutrino flavor oscillations. Signatures of neutrino oscillations in Super-Kamiokande (SK) might include distortion of the recoil electron energy ( $E_{\text{recoil}}$ ) spectrum, difference between the night-time solar neutrino flux relative to the day-time flux, or a seasonal variation in the neutrino flux. Observation of these effects would be strong evidence in support of solar neutrino oscillations independent of absolute flux calculations. Conversely, non-observation would constrain oscillation solutions to the solar neutrino problem. We describe here solar neutrino measurements from 1258 days of SK data.

SK, located at Kamioka Observatory, Institute for Cosmic Ray Research, University of Tokyo, is a 22.5 kton fiducial volume water Cherenkov detector that detects solar neutrinos via the elastic scattering of neutrinos off atomic electrons. The scattered recoil electron is detected via Cherenkov light production, allowing both the direction and total energy to be measured. These quantities are related to the original neutrino direction and energy. Detailed descriptions of SK can be found elsewhere [5, 9, 10, 11].

The 1258-day solar neutrino data were collected in four periods with different trigger thresholds between May 31, 1996 and October 6, 2000 (table I). The analysis threshold has been at 5.0 MeV except for the first 280 days where the data were analyzed with a threshold of 6.5 MeV. The analysis threshold is determined by the level of irreducible background events and the event trigger threshold. An event is triggered when the sum of PMTs registering a hit in a 200 nsec time window ( $N_{\text{hit}}$ ) is above a threshold (table I). This threshold should be sufficiently low that the trigger efficiency at the analysis threshold is nearly 100%. The lowering of the trigger threshold in periods 2–4 was made possible by the addition of a software filter to the data acquisition system that removes a large portion of background events. This removal is accomplished by reconstructing the event vertex and rejecting events with vertices within 2 m of the inner detector wall, most of which are due to external radioactivity. Each lowering of the trigger threshold in the course of the experiment was made possible by increasing the number of computers that run the filter program.

There are  $2.0 \times 10^9$  events in the raw data sample before background reduction. After removing cosmic ray muon events, the sample in the 22.5 kton fiducial volume with

Run period	$N_{\text{hit}}$ threshold	50/95% efficiency (MeV)	Analysis threshold (MeV)	Live-time (days)
(1) May 1996 ~	40.6	5.7 / 6.2	6.5	280
(2) May 1997 ~	34.5	4.7 / 5.2	5.0	650
(3) Sep. 1999 ~	30.4	4.2 / 4.6	5.0	320
(4) Sep. 2000 ~	27.7	3.7 / 4.2	5.0	8

TABLE I: The trigger and analysis thresholds and live-times during which they were used. The third column shows the recoil electron energy at which the trigger is 50% and 95% efficient. The software filter was added starting in May 1997.

energy between 5.0–20.0 MeV contains  $3.0 \times 10^7$  events. The dominant background sources in the low-energy region ( $E \lesssim 6.5$  MeV) are  $^{222}\text{Rn}$  in the water and external radioactivity; in the high-energy region ( $E \gtrsim 6.5$  MeV), radioactive decay of muon-induced spallation products accounts for most of the background. Background reduction takes place in the following steps: first reduction, spallation cut, second reduction, and external gamma-ray cut. The first reduction includes cuts that remove events due to electronic noise and arcing PMTs. In addition, a cut on the goodness of the reconstructed vertex is used to remove obvious background events originating from various non-physical sources. The number of remaining events after the first reduction is  $1.5 \times 10^7$ . The spallation cut has been improved compared to that used in earlier publications [5, 10, 11]. We have improved the likelihood functions used in removing spallation events and introduce a new cut for  $^{16}\text{N}$  events that originate from absorption of cosmic ray stopped  $\mu^-$  on  $^{16}\text{O}$ . The number of events in the high-energy region (6.5–20 MeV) before and after spallation cut is  $1.6 \times 10^6$  and  $3.3 \times 10^5$ , respectively. The spallation cut is 79% efficient for solar neutrino events. The second reduction removes events with poor vertex fit quality or with blurred Cherenkov ring patterns, characteristics of low-energy background events and external gamma rays. This newly introduced reduction step has improved the signal-to-noise ratio in the low-energy region by almost an order of magnitude. The number of events before and after the second reduction in the 5.0–6.5 MeV region are  $1.0 \times 10^7$  and  $1.4 \times 10^6$  events, respectively. In addition, the gamma-ray cut, which removes external events, has been tightened for those events with  $E < 6.5$  MeV. The combined efficiency of the first reduction, second reduction, and the external gamma ray cut for solar neutrino events is  $\sim 73\%$  for  $E \geq 6.5$  MeV, and  $\sim 52\%$  for  $E < 6.5$  MeV. After these reduction steps, 236,140 events remain in the fiducial volume above 5 MeV, with  $S/N \approx 1$  in the solar direction.

The SK detector simulation is based on GEANT 3.21 [12]. The energy scale was measured using a larger sample of data from an *in situ* electron linear accelerator [9] (LINAC) compared to that used in earlier results.

---

numerical values that were omitted from the PRL draft.

The detector simulation's reliability was tested using the well-known  $\beta$  decay of  $^{16}\text{N}$ , which is produced *in situ* by an  $(n, p)$  reaction on  $^{16}\text{O}$ . Fast neutrons for this reaction are produced using a portable deuterium-tritium neutron generator (DTG) [13]. The energy scale measured by the DTG agrees with that from the LINAC within  $\pm 0.3\%$ . The total systematic uncertainty in the absolute energy scale, including possible long term variation and direction dependence, is  $\pm 0.6\%$ .

We compare our solar neutrino measurements against reference fluxes and neutrino spectra in order to search for signatures of neutrino oscillations. For  $E_{\text{recoil}} \geq 5.0$  MeV, solar neutrinos are expected to come almost exclusively from the  $\beta$  decay of  $^8\text{B}$ , with a slight admixture of neutrinos from  $^3\text{He}$ -proton (*hep*) fusion. For the absolute flux of  $^8\text{B}$  and *hep* neutrinos, we take the BP2000 [6] SSM as our reference. The  $\beta$  decay spectrum of the  $^8\text{B}$  neutrinos is dominated by the transition to a broad excited state of  $^8\text{Be}$ , which decays immediately to two  $\alpha$  particles. Bahcall *et al.* [14] use a neutrino spectrum deduced from a comparison of world data on  $^8\text{Be}$   $\alpha$  decay [15, 16, 17] with the direct measurement of the positron spectrum from  $^8\text{B}$  decay measured by Napolitano, Freedman, and Camp [18]. Energy-dependent systematic errors are deduced from a combination of experimental uncertainties and the theoretical uncertainties in radiative and other corrections that must be made to convert the charged particle data into a neutrino spectrum [14]. Recently, Ortiz *et al.* [19] have made an improved measurement of the  $^8\text{B}$  spectrum based on  $^8\text{Be}$   $\alpha$  decay in which some of the major sources of systematic errors present in previous measurements were reduced or eliminated. We have adopted the neutrino spectral shape and experimental uncertainties from this measurement. These experimental uncertainties were then added in quadrature with the theoretical uncertainties given by Bahcall *et al.* [14].

The solar neutrino signal is extracted from the data using the  $\cos\theta_{\text{sun}}$  distribution (Fig. 1). The angle  $\theta_{\text{sun}}$  is that between the recoil electron momentum and the vector from the sun to the Earth. The solar neutrino flux is obtained by a likelihood fit of the signal and background shapes to the  $\cos\theta_{\text{sun}}$  distribution in data. The signal shape is obtained from the known angular distribution and detector simulation, while the background shape is nearly flat in  $\cos\theta_{\text{sun}}$ . In the  $^8\text{B}$  flux measurement, the data are subdivided into 19 energy bins in the range 5.0–20.0 MeV (binning as in Fig. 3). The likelihood function is defined as follows:

$$\mathcal{L} = \prod_{j=1}^{19} \frac{e^{-(Y_j \cdot S + B_j)}}{N_j!} \prod_{i=1}^{N_j} [B_j \cdot F_b(\cos\theta_i, E_i) + Y_j \cdot S \cdot F_s(\cos\theta_i, E_i)] \quad (1)$$

$S$  is the total number of signal events, while  $N_j$ ,  $B_j$ , and  $Y_j$  represent the number of observed events, the number of background events, and the expected fraction of signal events in the  $j$ -th bin, respectively.  $F_b$  and  $F_s$  are the probability for the background and signal events as a function of  $\cos\theta_{\text{sun}}$  and energy ( $E_i$ ) of each event. The

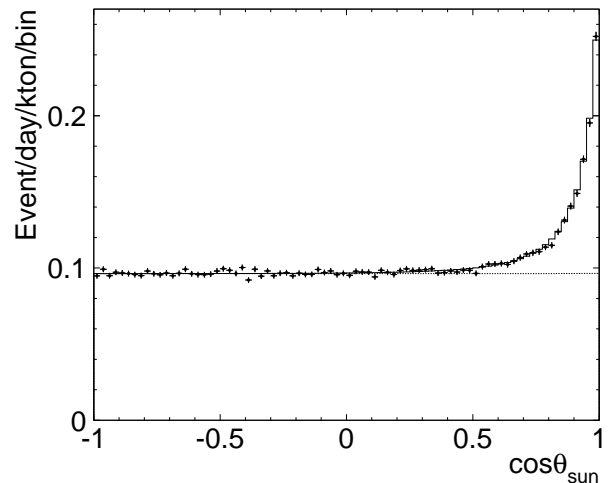


FIG. 1:  $\cos\theta_{\text{sun}}$  distribution for reconstructed energy  $E = 5.0\text{--}20.0$  MeV. The points represent observed data, the histogram shows the best-fit signal level plus background, and the nearly horizontal line shows the estimated background. The peak at  $\cos\theta_{\text{sun}} = 1$  is due to solar neutrinos.

likelihood function is maximized with respect to  $S$  and  $B_j$ . For the energy spectrum measurement, each term in the product over bins is maximized separately.

The best-fit value of  $S$  is  $18,464 \pm 204$  (stat.) $^{+646}_{-554}$  (sys.), which is  $45.1 \pm 0.5$  (stat.) $^{+1.6}_{-1.4}$  (sys.)% of the reference prediction. The corresponding  $^8\text{B}$  flux is:

$$2.32 \pm 0.03 \text{ (stat.)}^{+0.08}_{-0.07} \text{ (sys.)} \times 10^6 \text{ cm}^{-2}\text{s}^{-1}.$$

The total systematic error is  $^{+3.5\%}_{-3.0\%}$ , with the largest sources coming from the reduction cut efficiency ( $^{+2.2\%}_{-1.7\%}$ ), energy scale and resolution ( $\pm 1.4\%$ ), systematic shifts in the event vertex ( $\pm 1.3\%$ ), and the angular resolution of the recoil electron momentum ( $\pm 1.2\%$ ).

Fig. 2 shows the solar neutrino flux as a function of the solar zenith angle  $\theta_z$  (the angle between the vertical axis at SK and the vector from the sun to the Earth). Numerical values are shown in Table II. The day-time solar neutrino flux  $\Phi_d$  is defined as the flux of events when  $\cos\theta_z \leq 0$ , while the night-time flux  $\Phi_n$  is that when  $\cos\theta_z > 0$ . The measured fluxes are:

$$\begin{aligned} \Phi_d &= 2.28 \pm 0.04 \text{ (stat.)}^{+0.08}_{-0.07} \text{ (sys.)} \times 10^6 \text{ cm}^{-2}\text{s}^{-1} \\ \Phi_n &= 2.36 \pm 0.04 \text{ (stat.)}^{+0.08}_{-0.07} \text{ (sys.)} \times 10^6 \text{ cm}^{-2}\text{s}^{-1} \end{aligned}$$

Some neutrino oscillation parameters predict a non-zero difference between  $\Phi_n$  and  $\Phi_d$  due to the matter effect in the Earth's mantle and core [20]. The degree of this difference is measured by the day-night asymmetry, defined as  $\mathcal{A} = (\Phi_n - \Phi_d)/\Phi_{\text{average}}$ , where  $\Phi_{\text{average}} = \frac{1}{2}(\Phi_n + \Phi_d)$ . We find:

$$\mathcal{A} = 0.033 \pm 0.022 \text{ (stat.)}^{+0.013}_{-0.012} \text{ (sys.)}$$

Including systematic errors, this is  $1.3\sigma$  from zero asymmetry. Many sources of systematic errors cancel out

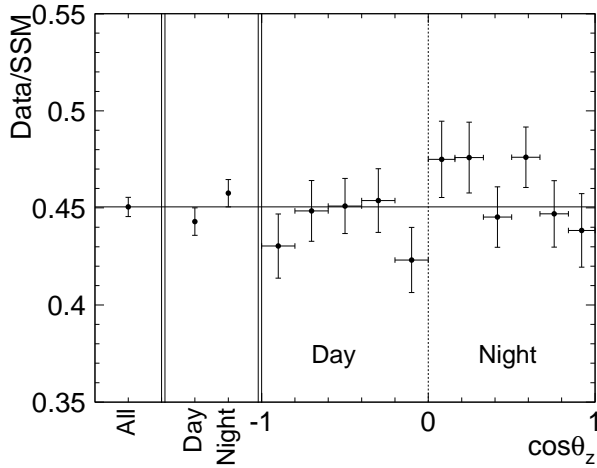


FIG. 2: The solar zenith angle ( $\theta_z$ ) dependence of the solar neutrino flux (error bars show statistical error). The width of the night-time bins was chosen to separate solar neutrinos that pass through the Earth's dense core ( $\cos \theta_z \geq 0.84$ ) from those that pass through the mantle ( $0 < \cos \theta_z < 0.84$ ). The horizontal line shows the flux for all data.

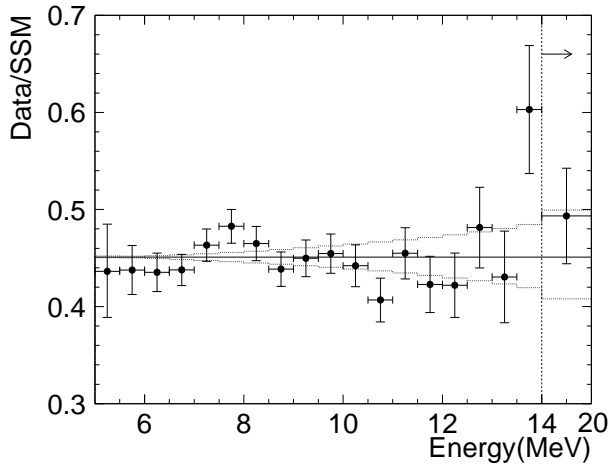


FIG. 3: The measured  $^8\text{B} + \text{hep}$  solar neutrino spectrum relative to that of Ortiz *et al.* normalized to BP2000. The data from 14 MeV to 20 MeV are combined into a single bin. The horizontal solid line shows the measured total flux, while the dotted band around this line indicates the energy correlated uncertainty. Error bars show statistical and energy-uncorrelated errors added in quadrature.

in the day-night asymmetry measurement. The largest sources of error in the asymmetry are the energy scale and resolution ( $^{+0.012}_{-0.011}$ ) and the non-flat background shape of the  $\cos \theta_{\text{sun}}$  distribution ( $\pm 0.004$ ).

Fig. 3 shows the measured recoil electron energy spectrum relative to the Ortiz *et al.* spectrum normalized to BP2000. (See Table III for numerical values.) A fit to an undistorted energy spectrum gives  $\chi^2/d.o.f. = 19.0/18$ . Energy-correlated systematic errors are considered in the definition of  $\chi^2$  [10]. The energy-correlated systematic

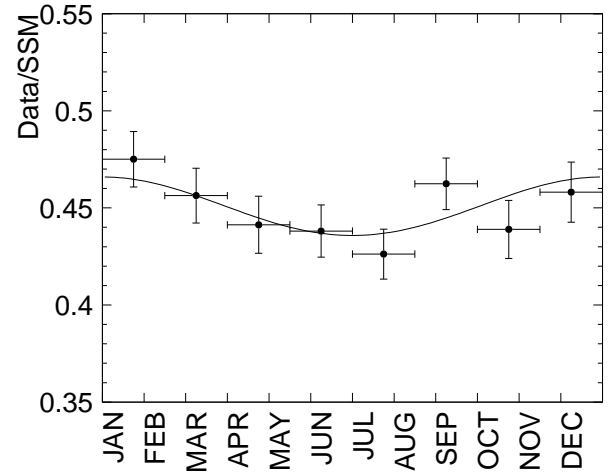


FIG. 4: Seasonal variation of the solar neutrino flux. The curve shows the expected seasonal variation of the flux introduced by the eccentricity of the Earth's orbit. Error bars show statistical errors only.

error (shown in Fig. 3 as a band around the total flux) is due to uncertainties that could cause a systematic shift in the energy spectrum. The sources of this error are uncertainties in the energy scale, resolution, and the reference  $^8\text{B}$  spectrum against which the data are compared.

The seasonal dependence of the solar neutrino flux is shown in Fig. 4. (See Table IV for numerical values.) The points represent the measured flux, and the curve shows the expected variation due to the orbital eccentricity of the Earth (assuming no neutrino oscillations, and normalized to the measured total flux). The data are consistent with the expected annual variation ( $\chi^2/d.o.f. = 3.7/7$ ). Systematic errors are included in the calculation of  $\chi^2$ . The total systematic error on the relative flux values in each seasonal bin is  $\pm 1.3\%$ , the largest sources coming from energy scale and resolution ( $^{+1.2\%}_{-1.1\%}$ ) and reduction cut efficiency ( $\pm 0.6\%$ ).

The *hep* neutrino flux given by BP2000 is  $9.3 \times 10^3 \text{ cm}^{-2} \text{ s}^{-1}$  [6], which is three orders of magnitude smaller than the  $^8\text{B}$  neutrino flux. Although the theoretically calculated *hep* flux is highly uncertain because of many delicate cancellations in calculating the astrophysical  $S$  factor, a recent calculation by Marcucci, *et al.* [21] shows that the flux is unlikely to be drastically larger than the value given in BP2000. The effect of *hep* neutrinos on solar neutrino measurements at SK is expected to be small. However, since the end-point of the *hep* neutrino spectrum is 18.77 MeV compared to about 16 MeV for the  $^8\text{B}$  spectrum, the high energy end of the  $E_{\text{recoil}}$  spectrum should be relatively enriched with *hep* neutrinos. An unexpectedly large *hep* flux may distort the  $E_{\text{recoil}}$  spectrum. In our measurement of the *hep* flux, we extract the number of events in the window  $E_{\text{recoil}} = 18\text{--}21 \text{ MeV}$  from a  $\cos \theta_{\text{sun}}$  distribution like the one shown in Fig. 1. This window was chosen because it optimizes the significance of the *hep* flux measurement in MC as-

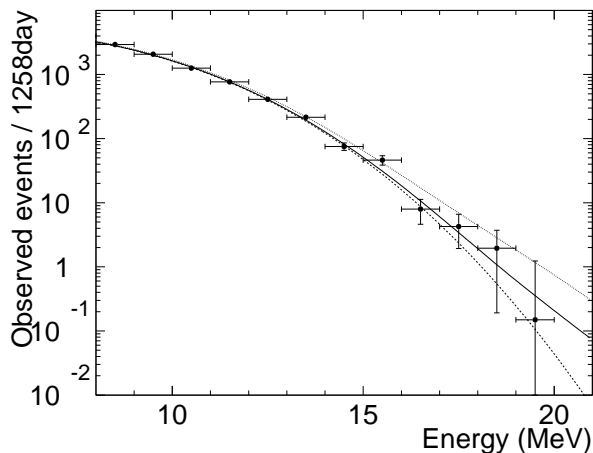


FIG. 5: Energy spectrum of recoil electrons produced by  $^8\text{B}$  and  $\text{hep}$  neutrinos, in 1 MeV bins. The points show data with statistical error bars. The curves show expected spectra with various  $\text{hep}$  contributions to the best-fit  $^8\text{B}$  spectrum. The solid, dotted, and dashed curves show the spectrum with 1, 4.3, and 0 times the BP2000  $\text{hep}$  flux, respectively.

suming BP2000  $^8\text{B}$  and  $\text{hep}$  fluxes. We find  $1.3 \pm 2.0$  events in the chosen window. Assuming that all of these events are due to  $\text{hep}$  neutrinos, the 90% confidence level upper limit of the  $\text{hep}$  neutrino flux is  $40 \times 10^3 \text{ cm}^{-2} \text{ s}^{-1}$  (4.3 times the BP2000 prediction). Fig. 5 shows the expected energy spectra with various  $\text{hep}$  contributions.

In summary, SK has lowered the analysis energy

threshold to 5.0 MeV, collected more than twice the data previously reported, and reduced systematic errors through refinements in data analysis and extensive detector calibrations. With those improvements, and with the 18,464 observed solar neutrino events, SK provides very precise measurements of the recoil electron energy spectrum, day-night flux asymmetry, and the absolute solar neutrino flux. The measured flux is  $45.1 \pm 0.5$  (stat.)  $^{+1.6}_{-1.4}$  (sys.)% of the BP2000 prediction. We found no statistically significant energy spectrum distortion ( $\chi^2/\text{d.o.f.} = 19.0/18$  relative to the predicted  $^8\text{B}$  spectrum), and the day-night flux difference of 3.3% of the average flux is  $1.3 \sigma$  from zero. However, the precision of these measurements should provide strong and important constraints on the neutrino oscillation parameters. The seasonal dependence of the flux shows the expected 7% annual variation due to the eccentricity of the Earth's orbit. This is the first neutrino-based observation of the Earth's orbital eccentricity. A stringent limit on the  $\text{hep}$  neutrino flux ( $\Phi_{\text{hep}} < 40 \times 10^3 \text{ cm}^{-2} \text{ s}^{-1}$ ) was obtained, which corresponds to 4.3 times the predicted value from BP2000.

The authors acknowledge the cooperation of the Kamioka Mining and Smelting Company. The Super-Kamiokande detector has been built and operated from funding by the Japanese Ministry of Education, Culture, Sports, Science and Technology, the U.S. Department of Energy, and the U.S. National Science Foundation. This work was partially supported by the Korean Research Foundation (BK21) and the Korea Ministry of Science and Technology.

- 
- [\*] Present address: Department of Physics, Massachusetts Institute of Technology, Cambridge, MA 02139, USA
  - [†] Present address: Korea Research Institute of Standards and Science, Yusong P.O. Box 102, Taejeon, 305-600, Korea
  - [‡] Present address: Department of Physics, University of Utah, Salt Lake City, UT 84112, USA
  - [§] Deceased.
  - [1] B. T. Cleveland *et al.*, *Astrophys. J.* **496**, 505 (1998).
  - [2] Y. Fukuda *et al.*, *Phys. Rev. Lett.* **77**, 1683 (1996).
  - [3] J. N. Abdurashitov *et al.*, *Phys. Rev. C* **60**, 055801 (1999).
  - [4] P. Anselmann *et al.*, *Phys. Lett. B* **327**, 377 (1994).
  - [5] Y. Fukuda *et al.*, *Phys. Rev. Lett.* **81**, 1158 (1998).
  - [6] J. N. Bahcall *et al.*, *astro-ph/0010346*.
  - [7] J. N. Bahcall, S. Basu, and M. H. Pinsonneault, *Phys. Lett. B* **433**, 1 (1998).
  - [8] S. Turck-Chièze and I. Lopes, *Astrophys. J.* **408**, 347 (1993).
  - [9] M. Nakahata *et al.*, *Nucl. Instrum. Methods Phys. Res. Sect. A* **421**, 113 (1999).
  - [10] Y. Fukuda *et al.*, *Phys. Rev. Lett.* **82**, 2430 (1999).
  - [11] Y. Fukuda *et al.*, *Phys. Rev. Lett.* **82**, 1810 (1999).
  - [12] GEANT Detector Description and Simulation Tool, *Cern Programming Library W5013* (1994).
  - [13] E. Blaufuss *et al.*, *Nucl. Instrum. Methods Phys. Res. Sect. A* **458**, 636 (2001).
  - [14] J. N. Bahcall *et al.*, *Phys. Rev. C* **54**, 411 (1996).
  - [15] D. H. Wilkinson and D. E. Alburger, *Phys. Rev. Lett.* **26**, 1127 (1971).
  - [16] B. J. Farmer and C. M. Class, *Nucl. Phys.* **15**, 626 (1960).
  - [17]  $\alpha$  energy spectrum measurement by L. De Braeckeleer and D. Wright. Unpublished. Quoted in L. De Braeckeleer, *et al.*, *Phys. Rev. C* **51**, 2778 (1995).
  - [18] J. Napolitano, S. J. Freedman, and J. Camp, *Phys. Rev. C* **36**, 298 (1987).
  - [19] C. E. Ortiz *et al.*, *Phys. Rev. Lett.* **85**, 2909 (2000).
  - [20] E. D. Carlson, *Phys. Rev. D* **34**, 1454 (1986); J. Bouchez *et al.*, *Z. Phys.* **C32**, 499 (1986).
  - [21] L. E. Marcucci *et al.*, *Phys. Rev. Lett.* **84**, 5959 (2000); L. E. Marcucci *et al.*, *Phys. Rev. C* **63**, 015801 (2000).

Day-Night	Zenith angle	Data/SSM	$\delta_i$
DAY	$-1 \leq \cos \theta_z \leq 0$	$0.443^{+0.007}_{-0.007}$	—
MAN1	$0 < \cos \theta_z \leq 0.16$	$0.475^{+0.020}_{-0.020}$	$+1.3\%$ $-1.2\%$
MAN2	$0.16 < \cos \theta_z \leq 0.33$	$0.476^{+0.018}_{-0.018}$	$+1.3\%$ $-1.2\%$
MAN3	$0.33 < \cos \theta_z \leq 0.50$	$0.445^{+0.016}_{-0.016}$	$+1.3\%$ $-1.2\%$
MAN4	$0.50 < \cos \theta_z \leq 0.67$	$0.476^{+0.016}_{-0.016}$	$+1.3\%$ $-1.2\%$
MAN5	$0.67 < \cos \theta_z \leq 0.84$	$0.447^{+0.017}_{-0.017}$	$+1.3\%$ $-1.2\%$
CORE	$0.84 < \cos \theta_z \leq 1$	$0.438^{+0.019}_{-0.019}$	$+1.3\%$ $-1.2\%$

TABLE II: Numerical results of the day/night analysis. The zenith angle region (2nd column), the ratio of observed and expected number of events (3rd column), and  $1\sigma$  error of systematic error (4th column). Systematic errors are relative to Day-flux. Energy range is 5.0–20.0 MeV.

Energy	Data/SSM			$\delta_{i,cor.}$	$\delta_{i,uncor.}$
(MeV)	ALL	DAY	NIGHT		
5.0-5.5	$0.436^{+0.046}_{-0.046}$	$0.438^{+0.065}_{-0.065}$	$0.434^{+0.063}_{-0.063}$	$+0.2\%$ $-0.2\%$	$+3.9\%$ $-3.1\%$
5.5-6.0	$0.438^{+0.024}_{-0.024}$	$0.428^{+0.034}_{-0.034}$	$0.446^{+0.034}_{-0.034}$	$+0.2\%$ $-0.2\%$	$+1.7\%$ $-1.6\%$
6.0-6.5	$0.435^{+0.019}_{-0.019}$	$0.426^{+0.027}_{-0.027}$	$0.444^{+0.027}_{-0.027}$	$+0.3\%$ $-0.3\%$	$+1.3\%$ $-1.4\%$
6.5-7.0	$0.438^{+0.015}_{-0.015}$	$0.431^{+0.021}_{-0.021}$	$0.444^{+0.021}_{-0.021}$	$+0.5\%$ $-0.6\%$	$+1.4\%$ $-1.4\%$
7.0-7.5	$0.463^{+0.015}_{-0.015}$	$0.462^{+0.022}_{-0.022}$	$0.464^{+0.022}_{-0.022}$	$+0.8\%$ $-0.8\%$	$+1.3\%$ $-1.4\%$
7.5-8.0	$0.483^{+0.016}_{-0.016}$	$0.494^{+0.023}_{-0.023}$	$0.472^{+0.022}_{-0.022}$	$+1.0\%$ $-1.1\%$	$+1.3\%$ $-1.4\%$
8.0-8.5	$0.465^{+0.017}_{-0.017}$	$0.452^{+0.023}_{-0.023}$	$0.477^{+0.023}_{-0.023}$	$+1.4\%$ $-1.3\%$	$+1.3\%$ $-1.4\%$
8.5-9.0	$0.438^{+0.017}_{-0.017}$	$0.402^{+0.024}_{-0.024}$	$0.473^{+0.024}_{-0.024}$	$+1.7\%$ $-1.7\%$	$+1.3\%$ $-1.4\%$
9.0-9.5	$0.450^{+0.018}_{-0.018}$	$0.454^{+0.026}_{-0.026}$	$0.446^{+0.025}_{-0.025}$	$+2.1\%$ $-2.0\%$	$+1.3\%$ $-1.4\%$
9.5-10.0	$0.455^{+0.019}_{-0.019}$	$0.449^{+0.027}_{-0.027}$	$0.460^{+0.027}_{-0.027}$	$+2.5\%$ $-2.3\%$	$+1.3\%$ $-1.4\%$
10.0-10.5	$0.442^{+0.021}_{-0.021}$	$0.430^{+0.029}_{-0.029}$	$0.454^{+0.029}_{-0.029}$	$+3.0\%$ $-2.7\%$	$+1.3\%$ $-1.4\%$
10.5-11.0	$0.407^{+0.022}_{-0.022}$	$0.386^{+0.030}_{-0.030}$	$0.426^{+0.032}_{-0.032}$	$+3.4\%$ $-3.2\%$	$+1.3\%$ $-1.4\%$
11.0-11.5	$0.455^{+0.026}_{-0.026}$	$0.439^{+0.036}_{-0.036}$	$0.470^{+0.037}_{-0.037}$	$+3.9\%$ $-3.6\%$	$+1.3\%$ $-1.4\%$
11.5-12.0	$0.423^{+0.028}_{-0.028}$	$0.455^{+0.042}_{-0.042}$	$0.394^{+0.038}_{-0.038}$	$+4.5\%$ $-4.2\%$	$+1.3\%$ $-1.4\%$
12.0-12.5	$0.422^{+0.033}_{-0.033}$	$0.389^{+0.045}_{-0.045}$	$0.455^{+0.047}_{-0.047}$	$+5.1\%$ $-4.8\%$	$+1.3\%$ $-1.4\%$
12.5-13.0	$0.481^{+0.041}_{-0.041}$	$0.514^{+0.061}_{-0.061}$	$0.451^{+0.055}_{-0.055}$	$+5.8\%$ $-5.4\%$	$+1.3\%$ $-1.4\%$
13.0-13.5	$0.431^{+0.047}_{-0.047}$	$0.468^{+0.070}_{-0.070}$	$0.397^{+0.063}_{-0.063}$	$+6.5\%$ $-6.2\%$	$+1.3\%$ $-1.4\%$
13.5-14.0	$0.603^{+0.065}_{-0.065}$	$0.551^{+0.092}_{-0.092}$	$0.653^{+0.094}_{-0.094}$	$+7.4\%$ $-7.0\%$	$+1.3\%$ $-1.4\%$
14.0-20.0	$0.493^{+0.049}_{-0.049}$	$0.430^{+0.067}_{-0.067}$	$0.559^{+0.071}_{-0.071}$	$+10.7\%$ $-9.5\%$	$+1.3\%$ $-1.4\%$

TABLE III: Numerical results of the energy spectrum analysis. The ratio of observed and expected number of events in all-time (2nd column), in day-time (3rd column), in night-time (4th column),  $1\sigma$  error of correlated systematic error (5th column), and  $1\sigma$  error of uncorrelated systematic error (6th column). Systematic errors are relative.

Time period	Data/SSM	Data/SSM at 1 AU	$\delta_i$
Jan. 1 – Feb. 16	$0.475^{+0.014}_{-0.014}$	$0.461^{+0.014}_{-0.014}$	$+1.3\%$ $-1.3\%$
Feb. 17 – Apr. 2	$0.456^{+0.014}_{-0.014}$	$0.450^{+0.014}_{-0.014}$	$+1.3\%$ $-1.3\%$
Apr. 3 – May 19	$0.441^{+0.015}_{-0.015}$	$0.446^{+0.015}_{-0.015}$	$+1.3\%$ $-1.3\%$
May 20 – Jul. 4	$0.438^{+0.013}_{-0.013}$	$0.451^{+0.014}_{-0.014}$	$+1.3\%$ $-1.3\%$
Jul. 5 – Aug. 19	$0.426^{+0.013}_{-0.013}$	$0.439^{+0.013}_{-0.013}$	$+1.3\%$ $-1.3\%$
Aug. 20 – Oct. 4	$0.462^{+0.013}_{-0.013}$	$0.469^{+0.014}_{-0.014}$	$+1.3\%$ $-1.3\%$
Oct. 5 – Nov. 18	$0.439^{+0.015}_{-0.015}$	$0.434^{+0.015}_{-0.015}$	$+1.3\%$ $-1.3\%$
Nov. 19 – Dec. 31	$0.458^{+0.016}_{-0.016}$	$0.445^{+0.015}_{-0.015}$	$+1.3\%$ $-1.3\%$

TABLE IV: Numerical results of the seasonal analysis. The time period (1st column), the ratio of observed and expected number of events without eccentricity correction (2nd column), the ratio of observed and expected number of events with eccentricity correction (3rd column), and  $1\sigma$  error of systematic error (4th column). Systematic errors are relative. Energy range is 5.0–20.0MeV.